WHITE PAPER

Advanced Electrochemical Impedance Spectroscopy (EIS) for Battery Testing

Measurement hardware, calibration, and electrochemical data interpretation

KEYSIGHT

This paper demonstrates reliable electrical testing and diagnostic evaluation of battery cells using advanced electrochemical impedance spectroscopy (EIS). Accurate EIS measurements are demonstrated using dedicated mechanical fixtures and electrical calibration schemes. The EIS results are put into the perspective of materials science, and together with circuit modeling, the main electrochemical parameters that are relevant to determine cell quality are derived. The new level of achieved accuracy leads to improved repeatability, robustness, and applications of EIS in the field of cell, module and pack testing.

Introduction to EIS

Lithium-ion batteries (LIB) are widely used in various applications due to their high energy and power density. The demand for rapid battery charging and high efficiency leads to continuous improvement in the cell chemistry and construction. Especially for automotive applications, the battery impedance (Z) has dropped to very low values. Today, battery impedance can be as low as few µΩs while the frequency range of interest is typically 1 mHz up to 10+ kHz. While LIB performance is continuously rising, the demand for high performance measurement equipment rises at the same time. Electrochemical impedance spectroscopy (EIS) is an established method providing insights into the electrochemistry and allowing to characterize the battery's parasitic circuit elements. EIS is typically done for battery R&D, for in-line cell manufacturing and for off-line quality control. Based on EIS data, among others, the state-of-charge (SOC) and state-of-health (SOH) can be quantitatively predicted using modeling procedures. This document presents EIS with a novel calibration workflow that allows for precise measurement of low battery impedances down to µΩ in a broad frequency range. Additionally, the calibrated data is used for equivalent circuit modeling and electrochemical interpretation, which is provided in the context of materials science and analytical electrochemistry.

Low Impedance EIS

Battery impedance in automotive applications has dropped to very low values - few µΩs, while the frequency range of interest is typically 1 mHz up to 10 kHz.

From dielectric spectroscopy to EIS

In materials science, dielectric spectroscopy is used for the direct measurement of the electrical properties of a material at high frequencies in the range of MHz…GHz. By comparing traditional dielectric spectroscopy and EIS with respect to the operating frequency, as shown in Figure 1, one gains a deeper insight into the capabilities of the methods themselves and on the materials science aspects.

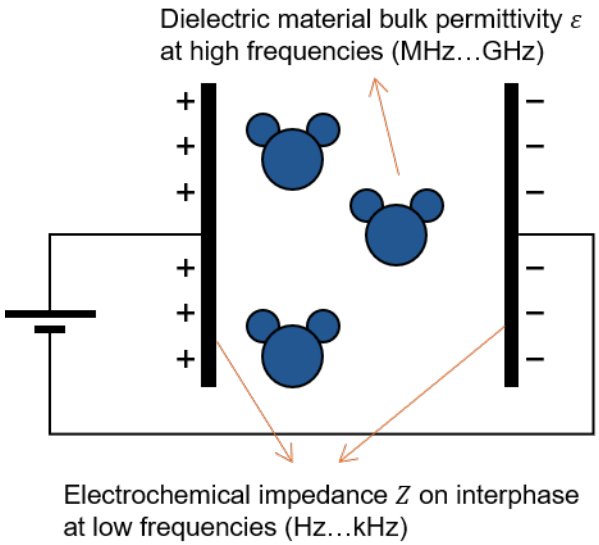

Figure 1. Dielectric and electrochemical processes

Dielectric properties include permittivity (which is a measure for storing electrical energy) and conductivity (which is a measure for transferring electrical charges). There are various instruments to measure dielectric spectroscopy in the MHz and GHz frequency range employing an impedance analyzer or network analyzer, respectively. For instance, the Keysight dielectric probe-kit measures the materials properties in a broad frequency range of 10 MHz to 50 GHz [1]. The two parameters measured by dielectric spectroscopy, permittivity and conductivity, are both related to molecular properties. For example, a dielectric is a material whose capacitive current (out of phase) exceeds its resistive (in phase) current. An ideal dielectric is an insulator with no free charges that are capable of storing electrical energy. The dielectric analysis presents permittivity and conductivity as a combined complex permittivity ε^*, with $\varepsilon^* = \varepsilon' - j \cdot \varepsilon''$, and ε' being the real permittivity or dielectric constant related to the energy storage and alignment of dipoles, while ε'' is the imaginary permittivity or loss factor related to the ionic conduction. The dielectric response is based on the concept of energy storage and resulting relaxation, which is the time required for dipole molecules to reversibly orient themselves in the external AC electric field. The frequency dependence of dielectric materials, such as the capacitance, permittivity, and conductivity can be described with the Debye model of single relaxation frequency. Traditionally, dielectric analysis has been applied to the analysis of bulk dielectric properties of polymers, plastics, composites, non-aqueous fluids and often operated above 1 MHz frequency (a good overview can be found in the textbook [2]).

A similar concept is used in EIS with the main difference to dielectric spectroscopy that the frequencies are lower (mHz…kHz) and the data analysis is based on complex impedance $Z^* = Z_{real} + j \cdot Z_{imag}$. Thereby, the imaginary permittivity ε'' is related to the inverse of Z_{real} while the real permittivity ε' is related to the inverse of Z_{imag}. EIS is investigating charge and electrochemical kinetic processes that occur at electrode sample interfaces, and particularly at low frequencies down to mHz. Unlike dielectric spectroscopy, the impedance analysis is based not on bulk material investigations but rather on interfacial impedance parameters, including Faradaic and double layer interfacial kinetics and the effects of DC potential modulation. In summary, interfacial polarization is studied with EIS at low frequencies, while solution effects are studied in dielectric spectroscopy at high frequencies (a good overview can be found in the textbook [3]).

EIS measurement principles

A typical EIS measurement system consists of the measurement hardware, the software to control the hardware and to calculate the impedance, a fixture to connect the device under test (DUT), as well as cables and connectors, as shown in Figure 2. EIS measurements are performed by applying an alternating current (AC) signal (galvanostatic mode) or AC voltage signal (potentiostatic mode) to the DUT and recording the system response, which is the voltage drop V across the DUT terminals and the current I through the DUT, respectively.

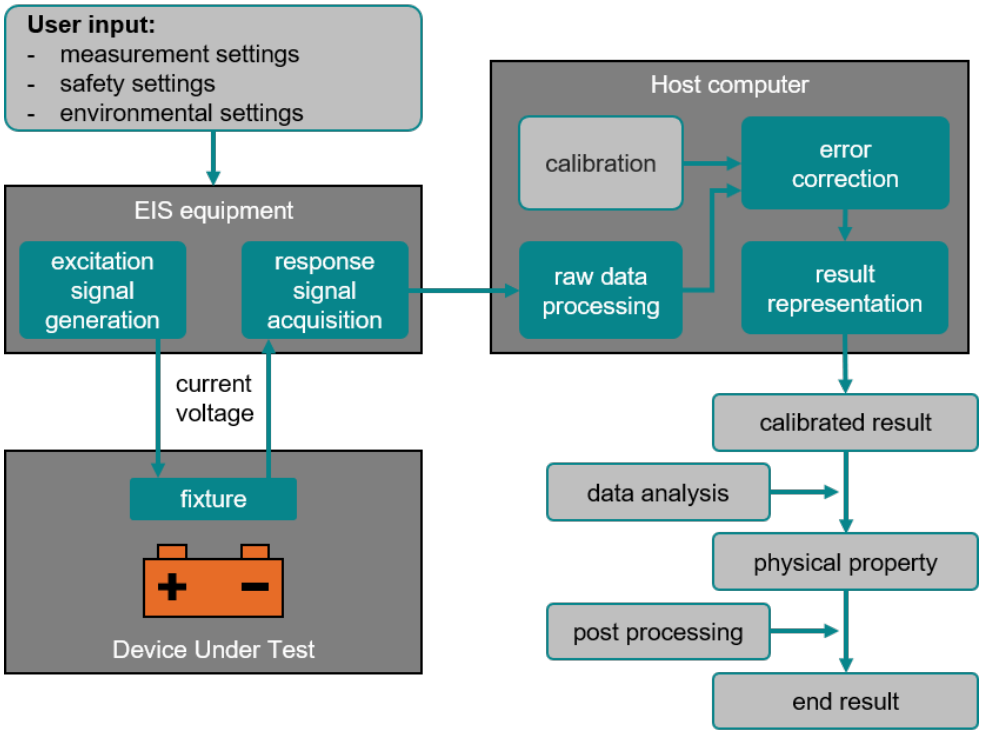

Figure 2. Basic block diagram of EIS including hardware, software, calibration and data analysis

The excitation signal generation block comprises of a signal waveform generator and a power amplifier that provides the desired voltage or current amplitude to stimulate the DUT. The EIS equipment is connected to the DUT by a four-wire Kelvin connection that allows for separate sensing of the response voltage. The current and voltage signals are processed and digitized in the response signal acquisition block and streamed to a host computer where the data processing is performed. The frequency $\omega = 2\pi f$ of the excitation signal is swept within a defined frequency window. For each frequency of interest, the phase difference φ between the current and voltage signal, as well as their amplitudes, are calculated (see Figure 2). These values are then used to compute the complex raw impedance $Z(\omega) = \frac{u_A}{i_A} e^{j\varphi}$ in Ohm. After applying error correction, the calibrated end result is available for further analysis.

The impedance Z can be visualized either by representing the magnitude $|Z|$ and the phase $\varphi(Z)$ as a function of the frequency in the form of a Bode diagram, or can be plotted in a complex plane with the frequency as independent parameter and equal axis scaling for real $Re(Z)$ axis and imaginary $Im(Z)$ axis. This type of plot is called a Nyquist plot and in electrochemistry it is common practice to swap the sign of the imaginary part (i.e. to plot the complex conjugate of the data), as shown in Figure 3 [4].

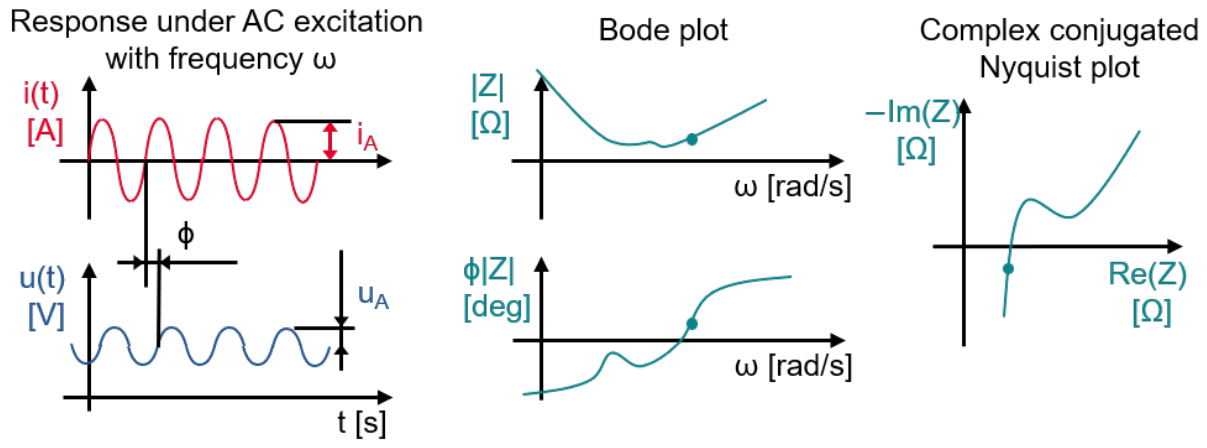

Figure 3. Excitation signal and representation of the complex impedance

Electrochemical interface model for EIS

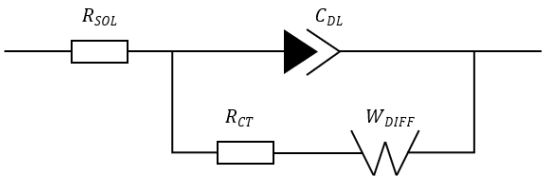

Figure 4. Randles equivalent circuit

The example of the Randles circuit, shown in Figure 4, is broadly used as the initial impedance model of a simple electrochemical reaction mechanism in a cell [5]. The highly conductive ionic bulk solution has a bulk impedance that is low and can be represented by a purely resistive element R_{SOL}. After passing through the solution resistance element, the current has to cross the interface where the charge transfer exchange between the solution ions and electrons in the electrodes take places. This process is controlled by the kinetic process represented by a charge-transfer resistance R_{CT}. Deposition of ion charges at the electrolyte interface is countered by electronic charges of the opposite sign on the electrode interface, establishing a 'double-layer capacitance' C_{DL}. At relatively high frequencies around 1 kHz the system impedance is practically all resistive and dominated by R_{SOL}. At lower frequencies around 1…100 Hz the interfacial kinetic processes represented by $C_{DL}||R_{CT}$ dominate and the system impedance is largely affected by the double layer capacitance C_{DL} element and the charge-transfer resistance R_{CT}. The characteristic frequency is $f_C = 1/2\pi R_{CT} C_{DL}$. An ideal semicircle in the Nyquist plot is an indication of the activation-energy controlled charge transfer process, while a depressed semicircle is an indication of multiple processes with similar relaxation time constants or distributed non-ideal kinetics. Additionally, several non-ideal circuit elements are used to better describe experimental results, including the constant phase element (CPE) and the Warburg diffusion impedance W_{DIFF}. The CPE is used as modified capacitor, while the Warburg element is used to describe materials diffusion at the electrode interface. There are several physical processes (electrode porosity and surface roughness, variability in electrode conductivity, grain boundaries) responsible for the deviations from ideal resistor and capacitor response that require a CPE representation [2] [3].

Accurate EIS Measurements

EIS fixturing

A proper connection between the EIS instrument and the fixture must be ensured because the fixtures and the wires influence the measurement accuracy. The cables are firmly connected to the instruments and have a stable position, because moving cables can lead to a change in the measured impedance, especially for low impedance values. Figure 5-a shows that the excitation signal is provided by the EIS 'force' terminal while the current over the DUT is measured. The resulting voltage drop at the DUT terminals is sensed by individual contacts in the test fixture (i.e. 4-wire connection) which are connected to the equipment 'sense' terminal. Twisted pair wiring for both force and sense connections minimizes mutual magnetic coupling and reduces systematic and random errors arising from cables significantly. Note that the test fixture should be specifically designed for each battery form factor. The accuracy of low impedance battery EIS measurements depends strongly on the spatial position of the DUT in relation to the test fixture. Figure 5-b shows how different DUT positions with respect to the measurement plane lead to different current paths. The measurement plane is defined by the 'short' calibration standard. The different DUT positions lead to different current paths and thus they lead to changes in mutual magnetic coupling and losses due to eddy currents in conductive structures.

The latter two effects have a strong influence on the impedance at higher frequencies (typically 1 kHz … 10 kHz). During the experiments the following empirical and phenomenological estimation was observed:

$$|\overrightarrow{\Delta x}| = \frac{10^5 |\Delta Z_{max}(f_{max})|}{f_{max}}$$

with the maximum frequency f_{max} [Hz] and the maximal acceptable absolute impedance change $|\Delta Z_{max}(f_{max})|$ [Ω] provides a practical estimation of the required position accuracy.

The absolute spatial error vector $|\overrightarrow{\Delta x}|$ is given in millimeters and describes the acceptable variation of the DUT in relation to the calibration plane. For instance, an absolute repeatability error lower than 100 µΩ at 10 kHz requires typically a position accuracy of better than 1 mm in all three dimensions.

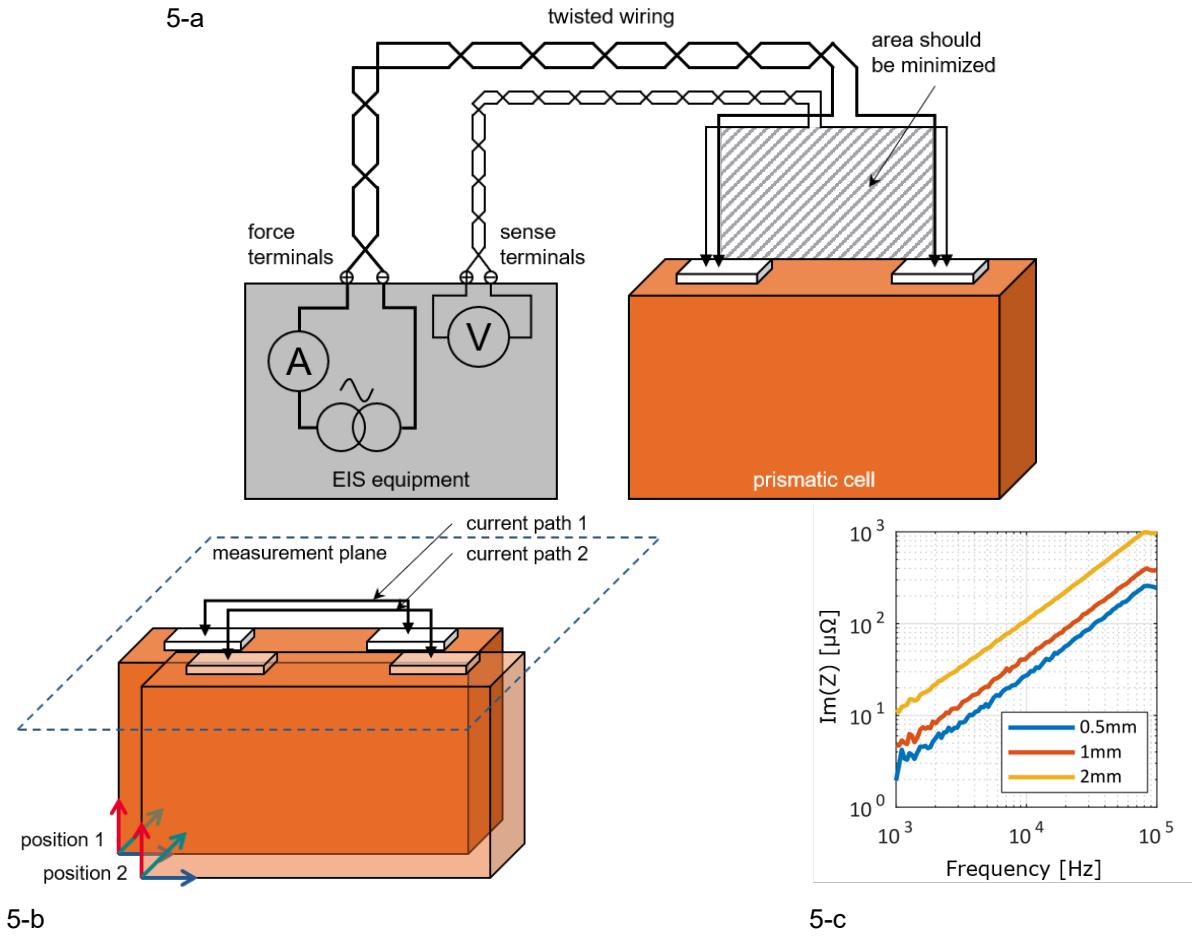

Figure 5. Fixture wiring and accuracy.

(5-a) Twisted wiring diagram including force and sense terminals, as well as four-wire connection.

(5-b) Relative position of the DUT with respect to the measurement plane.

(5-c) Imaginary impedance difference over frequency for three different positions in x-direction with respect to a reference position

A measurement example is given in Figure 5-c where the differences in the imaginary part of the impedance are shown for a 1 mΩ verification standard that has been misaligned in x-direction by 0.5 mm, 1 mm, and 2 mm, respectively. The misalignment increases the non-coaxial area and therefore the inductance. In general, random errors can be minimized if the following points are considered adequately:

- The test fixture should be mechanically rigid and stable, and a position guide should accurately define the position of the DUT as well as the position of the calibration standards in all three dimensions.
- The calibration standards should be of low drift and fit mechanically to the test fixture and resemble the DUT from a current path perspective.
- A defined contact pressure should be ensured on the contacts that interface the test fixture and the DUT. For example, spring loaded contacts can be used or screw terminals can be tightened up to a defined torque.
- The instrument's noise and drift need to be considered. Random thermal noise typically occurs at frequencies above 1…10 Hz and can be reduced by narrowband measurements and averaging, at the cost of longer measurement times. Instrument drift is especially relevant for very low frequency measurements, e.g. 1 mHz.
- A settled constant ambient temperature and a suitable warm up period are recommended. Thermal contact voltages can introduce a constant offset voltage. However, this does not affect the EIS results since the measurements are done at AC signals. Only at very low frequencies errors could arise if the equipment temperature changes during one measurement cycle.

EIS calibration

Before the DUT is measured, a calibration process is performed. In general, the accuracy of an EIS measurement is limited by systematic and random (stochastic) errors. While systematic errors can be corrected by calibration and correction methods, random errors like system noise and fixture repeatability cannot be corrected. Several calibration workflows of different complexity and accuracy level are available, ranging from simple offset subtraction with a short measurement to full calibration with three-term methods where three well-known standards are used. The calibration process is used to determine the systematic (repeatable) errors that are added by the equipment to the measurement result. In a subsequent correction step the calibration is used to correct the actual DUT measurements. For this, an error model is defined, and the calibration standards are measured to obtain the error coefficients. It is important to use calibration standards specifically designed for the fixture in use. Here, a calibration method employing three calibration standards including a short and two resistors of known values (resistance and inductance) is used, working over the full frequency spectrum in EIS.

The term 'calibration' describes the process of determining the systematic errors of a measurement device. The term 'correction' describes the process of removing the systematic errors from an actual measurement, thus resulting in a more correct result. In EIS, the quantity that is measured is the impedance which is the ratio of voltage and current. To calibrate an impedance meter a known standard impedance is required. The question where the standard impedance is coming from leads to the topic of traceable metrology. Impedance metrology is based on impedance standards that are typically preserved in national metrology institutes (NMIs). For instance, the Ohm-standard is currently derived from the quantum Hall effect with an accuracy of 10^{-6}. Standards at various impedance levels for both DC and AC are derived by comparison methods including bridge circuits and nulling techniques. Those standards are used in calibration laboratories as primary standards. Based on primary standards, working standards are then derived which are eventually used for instrument calibrations. If each step of an instrument calibration can be traced towards the primary standard, the calibration is called 'traceable'.

Figure 6 provides a general overview of the calibration and correction workflow used in Keysight EIS equipment. The upper part shows the calibration process, during which known impedance standards (i.e. working standards) are measured. In Figure 6 these are a short, a 10 mΩ and a 100 mΩ shunt. Each of the impedance standards has a known frequency dependent complex impedance response that is stored in a corresponding standard definition dataset together with the uncertainty. This definition dataset has been determined by comparing the working standard against a traceable primary standard in a factory calibration. The measured raw data together with the definition data are used to solve the error model for the frequency dependent complex error coefficients. The two lower Nyquist plots in Figure 6 show the effect of the correction for a 25 Ah prismatic Li-Ion cell. The corrected data shows a different behavior at higher frequencies indicating less inductance. The complexity of the error model can vary, depending on the EIS hardware, the impedance range, and the accuracy requirements.

EIS calibration

Three independent standard measurements are required to solve the corresponding equation system and typically, one short-standard and two resistive shunt-standards are used.

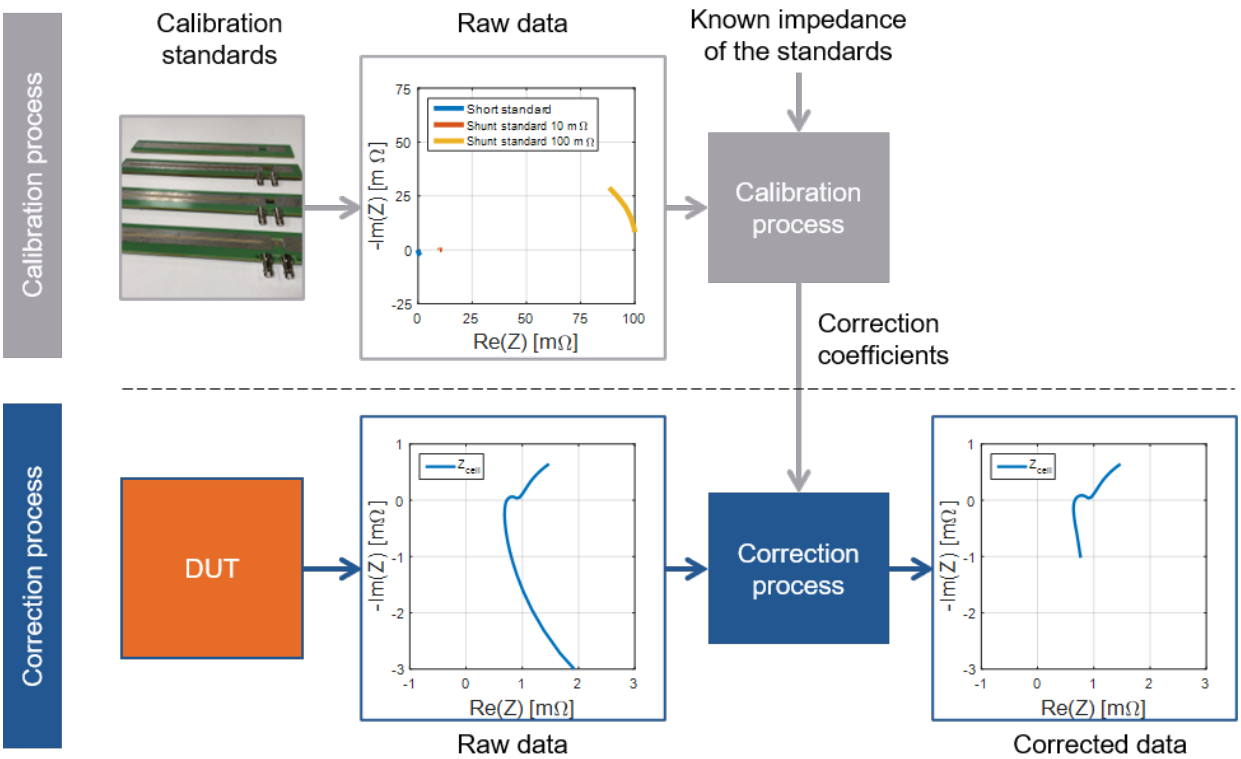

Figure 6. Calibration and correction workflow for EIS measurements, shown on the example of a 25 Ah prismatic Li-Ion cell.

Here the most general three term error model is used, which covers a wide impedance range and provides a full correction of the systematic error. The model implements a so-called conformal map that preserves the local angle between two vectors in the raw data domain and the corrected data domain. For example, the 90-degree phase angle between a resistor and a capacitor is never changed by the calibration method. Three independent standard measurements are required to solve the corresponding equation system and typically, one short-standard and two resistive shunt-standards are used. The shunt values should thereby cover the impedance range of the battery cells that are measured subsequently (for example 10 mΩ and 100 mΩ). The lower part of Figure 6 shows the correction workflow. The DUT is measured and the resulting raw data is fed together with the error coefficients into the correction equation. The correction equation is derived by mathematical conversion from the error model. While the calibration process involves three measurement steps and the solving of an equation system, the correction process is a straightforward application of one equation to one set of measurement data. The mechanical and electrical construction details of the standards have a significant effect on the corrected impedances particularly at higher frequencies. For instance, the imaginary part at higher frequencies is dominated by the inductance of the battery cell which is a pure geometrical effect. Typical cells (for example prismatic or pouch cells) have spatial dimensions in the centimeter range and inductance values in the range of 50…500 nH. This inductance values need to be interpreted with respect to the reference geometry that is mainly defined by the short standard which should be a highly conductive, low loss connection between the two terminals of the test fixture. A comprehensive review is given by [6].

EIS measurement hardware

The signal generation and measurement equipment needed to perform the EIS measurements is readily integrated within the Keysight battery test systems (BTS). This allows using the same equipment both for the high current charging/discharging, cycling and pulse tests, as well as for high-precision measurements such as EIS and cyclic voltammetry. Figure 7 shows a screenshot of the control software Energy Storage Discover (ESD), when used to measure the impedance spectrum of a cell at different SOCs. The left side shows the test sequence; the middle portion shows recorded current and voltage where the alternating charge and EIS-test steps are clearly visible; on the right side are shown the impedance spectra for the different SOC as Bode and Nyquist diagrams.

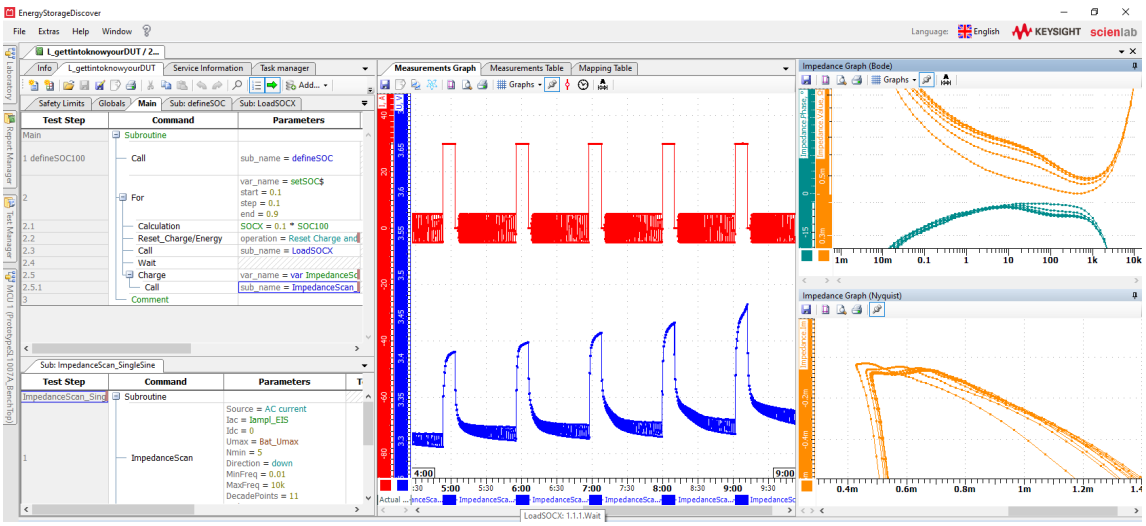

Figure 7. Energy Storage Discover (ESD) control software, used for EIS tests at different SOCs.

Examples of Keysight battery test equipment are shown in Figure 8. The battery test laboratory in Figure 8-a has climate chambers, where the tested cells can be placed, and separate cabinets holding the battery test equipment – electronic amplifiers that can control the current, the voltage or the power over the cell. Figure 8-b shows a so called “Combined Battery Test Solution” (CBTS), where the climate chamber (front side) and the electronic amplifiers (back side) are integrated in the same cabinet. Note that in the picture the door of the right-hand side climate chamber has been removed to show the fixtures for contacting the battery cells. The advantages of such a CBTS approach are the reduced footprint for the equipment in the laboratory, the short (in cabinet) connection between the power electronics and the cells, and the improved shielding against external electromagnetic effects. The advantages of the approach in Figure 8-a are the high modularity and flexibility of the system, as well as the possibility to match the battery test power electronics with different climatic, temperature and storage chambers.

8-a

8-b

Figure 8. Keysight battery test systems.
(8-a) in a test lab with climate chambers.
(8-b) as cabinet system integrating climate chamber and electronic amplifiers.

Depending on the cell form factor, different cell fixtures and in turn also different calibration standards are available from Keysight for doing accurate EIS, as shown in Figure 9. Additionally, as with the form factor also the cell capacity and impedance change, the requirements on the EIS equipment change as well, as shown in Table 1.

Property	Coin cells	Pouch cells	Prismatic cells
Capacity	<mAh … 100mAh	1 Ah … 30 Ah	10 Ah … 100 Ah
Impedance range |Z|	1 Ω … 1 kΩ	10 mΩ … 1 Ω	100 µΩ … 10mΩ
EIS test current (rms)	1 mA … 10 mA	100 mA … 5 A	1 A … 10 A
EIS impedance resolution	~10 mΩ	~1 mΩ	~10 µΩ

Table 1. Typical cell and EIS characteristics for different cell form factors

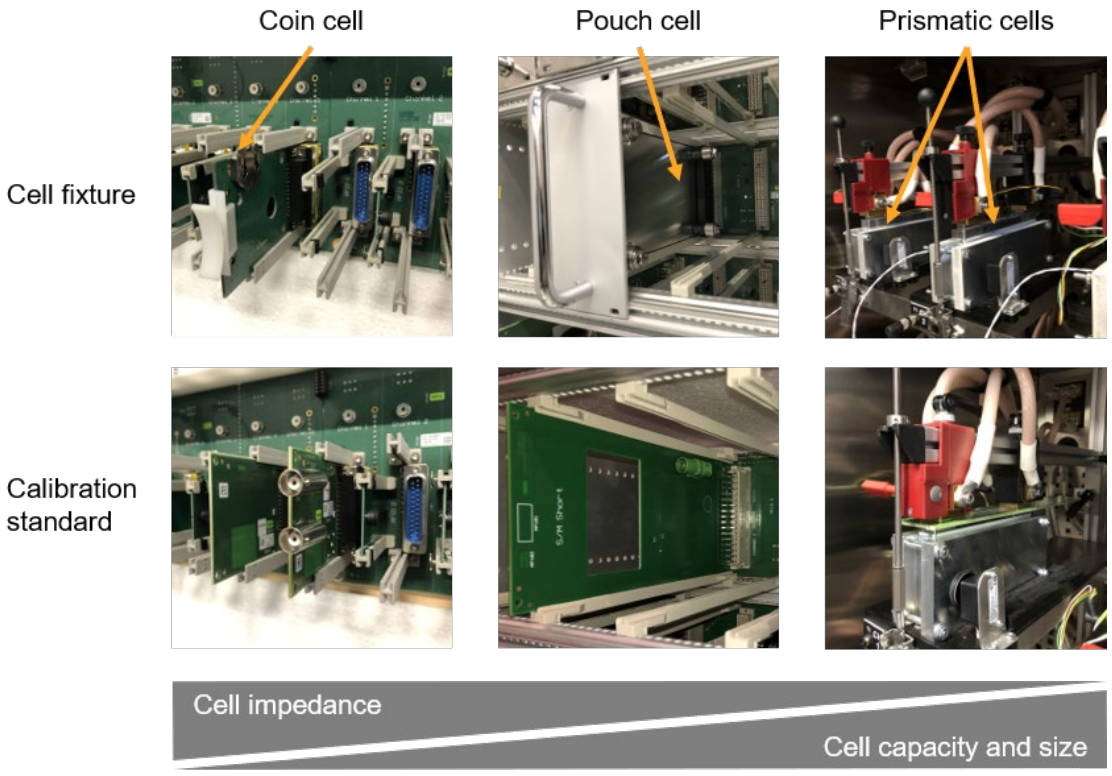

Figure 9. Cell fixtures and calibration standards for coin cells (left column), pouch cells (center column), and prismatic cells (right column).

IS Results and Data Interpretation

EIS results and data fitting with equivalent circuit model

Figure 10 shows the measured EIS plots of two commercial cells in the frequency range of 10 mHz to 10 kHz, including a cylindrical cell (Figure 10-c) and a prismatic cell (Figure 10-d). The EIS data is calibrated as described above. For fitting the experimental EIS data the model shown in Figure 10-a was used, representing a modified Randles circuit, summarized as $L + R_{SOL} + [R_{SF}||C_{SF}] + [R_{CT}||C_{CT}] + \sigma_W$ [5].

A proprietary EIS fitting software was developed in Keysight that was used for robust and automatic fitting of EIS curves. Here two resonant elements in series were used, resulting in two semicircles (Z_{ARC}) that are significantly overlapping. From left to right the extended Randles equivalent circuit includes a wiring inductance L describing at high frequencies (>1 kHz) the effect of wiring and electrode connections to the current collectors. At roughly 1 kHz, the resistance of the electrolyte (R_{SOL}) is related to the point where the imaginary part of the impedance reaches zero. A first semicircle (Z_{ARC1}) describing the surface film resistance (R_{SF}) and surface film capacitance (C_{SF}) is obtained from the best fit, corresponding to the electrolyte interphase and Lithium migration through the surface films.

10-a

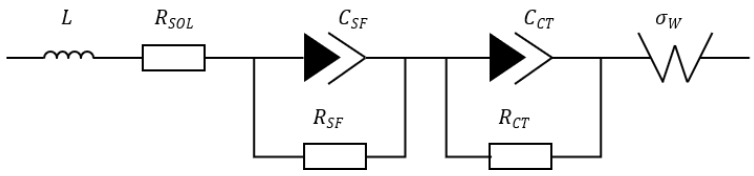

10-b

Parameter	L	R_{SOL}	R_{SF}	C_{SF}	R_{CT}	C_{CT}	σ_W
Unit	nH	Ω cm²	Ω cm²	µF / cm²	Ω cm²	µF / cm²	m Ω s$^{1/2}$
cylindrical cell	326	7.6	0.83	9570	1.98	290	2.31
prismatic cell	109	3.4	0.88	1302	1.35	456	0.091

10-c

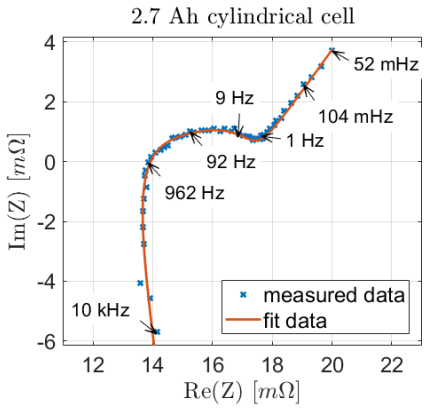

10-d

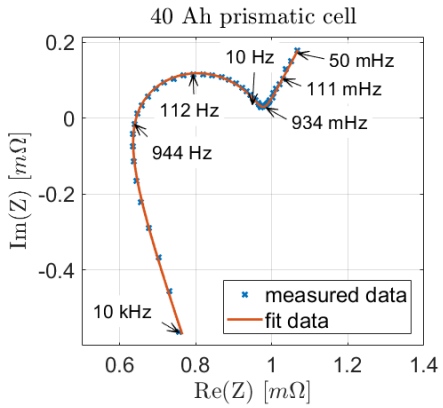

Figure 10. Calibrated EIS data and fitting to an equivalent circuit model.

(10-a) Equivalent circuit model used for calculating the electrochemical fit parameters, including two Z_{ARC} elements for surface film (e.g. R_{SF}) and charge-transfer (R_{CT}).

(10-b) Values of the 7 fit parameters are given for both the cylindrical (effective electrode surface of A_{eff}=600 cm²) and the prismatic cell (A_{eff}=6300 cm²).

(10-c) Impedance plot for a 2.7 Ah cylindrical cell and (d) for a 40 Ah prismatic cell, where the measurement frequencies range from mHz to 10 kHz.

A second semicircle (Z_{ARC2}) at lower frequency describes the charge transfer resistance between the electrolyte and the solid surface (R_{CT}) as well as the double layer capacitance (C_{CT}). Both semicircles are significantly overlapping between 1 Hz and 1 kHz.

At the apex of the semicircles the capacitive behavior is the strongest and the double layer capacitance values can be determined. The Warburg impedance is then in series to the two Z_{ARC} elements, giving the linear low-frequency region of the spectra (< 1 Hz) that is characteristic to the materials diffusion processes at the solid-state electrode. Thereby, σ_W describes the Warburg coefficient that is directly related to the diffusion coefficients of the oxidized (D_{Ox}) and the reduced (D_{Red}) electroactive species. As such, in contrast to the basic Randles circuit, the modified model describes the surface film and charge transfer resistance separately [2], [3]. The seven fit parameters resulting from this model are given in Figure 10-b both for the cylindrical cell and the prismatic cell. The electrochemical fit parameters are described in more detail in the next section. The exact values of the parameters depend on the cell SOC, the cycling number, or more generally, on the SOH of the cell. Typically, after several charge/discharge

cycles of a battery, the surface film and charge transfer resistance values increase because of aging and capacity fading. Smaller surface film resistances are related to improved electrolyte interphase layers, including the SEI on the anode and the typically less investigated cathode interface layer.

EIS data interpretation

For the interpretation of EIS measurements there are typically seven characteristic items describing the various effects within of the cell, including the electrochemical processes, the double layer capacitance, and the mass transport diffusion [5] [2] [3]. The seven parameters can be related to a specific chemical or physical process within the cell, and as such they can be used to determine the SOH of the cell. As depicted in Figure 11, the seven parameters appear at different frequencies in the EIS plot and can thereby be well distinguished. Note that the given frequency ranges are exemplary and will vary depending on the cell chemistry, form factor and capacity.

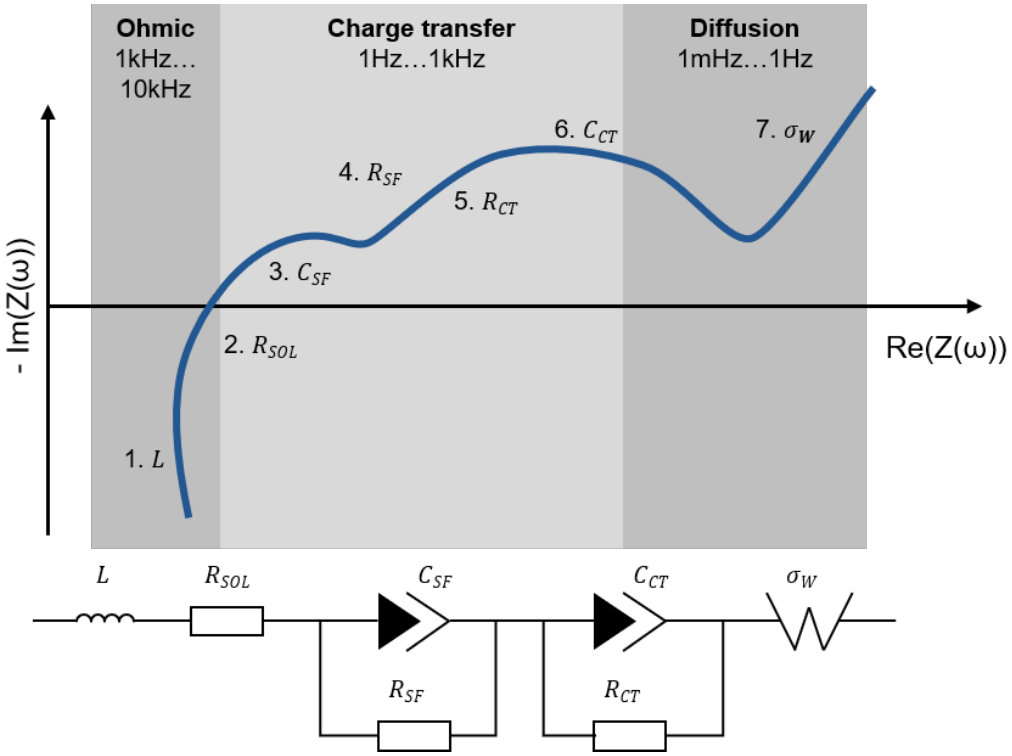

Figure 11. Characteristic parameters of equivalent circuit model of a battery cell.

1. L – High frequency inductive behavior in wires and electrodes

L describes the high frequency (typically >1 kHz) inductive behavior of uncompensated impedances in wires and electrodes. By using accurate mechanical fixtures and minimizing the inductive wire loops various effects of electrical contact quality and electrode surface porosity can be obtained from L.

2. R_{SOL} – Bulk media solution resistance

R_{SOL} describes the bulk media conduction and it is typically measured at 1 kHz frequency, with $R_{SOL} \sim 1/\sigma$, where σ is the conductivity of the electrolyte. Assuming a standard water salt electrolyte, for a working electrode with an area $A = 1$ cm², a separation to the counter electrode of $d = 0.1$ cm and a measured impedance $|Z| = 1\ \Omega$, the conductivity can be estimated [2] to:

$$\sigma = \frac{d}{Z \cdot A} = \frac{0.1\ cm}{1\ \Omega \cdot 1\ cm^2} = 10\ S/m$$

3. C_{SF} – Electric charging of the electrochemical surface film

4. R_{SF} – Surface film adsorption on electrode

The surface-film resistance R_SF includees adsorption/desorption processes appearing around 100 Hz… 1 kHz. It is in parallel with the surface-film capacitance C_{SF} and forms the electrochemical sorption impedance, which depends on charges associated with specific adsorption or desorption processes, the thickness and dielectric material properties of the layer. It includes anodic SEI effects but also cathode interface layers. Typically, it results in a distortion of the main semicircle or in an additional arc appearing at a higher frequency compared to the charge-transfer resistance semicircle.

5. R_{CT} – Faradaic electron transfer near the electrode surface

6. C_{CT} – Electric charging of the electrochemical double layer capacitance

The ideal double-layer capacitance C_{CT} is typically replaced by a CPE_{CT}, and the double-layer capacitance charging typically occurs between 1…500 Hz in conductive solutions with values of around $C_{CT} = 10 \ldots 500$ µF/cm2. The charge-transfer resistance R_{CT} describes the main redox reaction in the cell. The charge-transfer reaction is controlled by the Faradaic response which is the rate of electron transfer to the electroactive species in the electrolyte occurring near the electrode surface in the double layer with a thickness of around 1…10 nm. The kinetic-rate constant k_0 can be expressed as a function of R_{CT} at the electrode. Kinetic-rate constants governing electron transfer depend exponentially on the applied potential and the corresponding standard electrochemical potential and are therefore depending on the overpotential. At high overpotentials, R_{CT} becomes independent of the external potential and the electrode process will not be limited by the electrochemical kinetics.

7. σ_W – Mass transport from the bulk solution to the electrode surface, Warburg diffusion

The diffusion resistance Z_{DIFF} to current flow carried by electroactive species can create impedance, known as the Warburg element, W_{DIFF}. The mass transport Warburg diffusion σ_W governs the impedance around 1 mHz…1 Hz. The diffusion layer thickness can reach in bulk electrolytes from 0.1 mm at 100 Hz to 1 mm at 0.01 Hz, and for thin samples may extend all the way to the counter electrode and becomes comparable to the overall sample thickness. For standard batteries, typically the diffusion happens in the

solid state at the electrode surface layer with around 100 nm…100 µm diffusion thickness. The Warburg coefficient σ_W can be determined from the slope of the impedance plot, with Z vs. $\omega^{-1/2}$ resulting in typical values of few mΩs$^{1/2}$ and typical diffusion coefficient of 10^{-9} cm^2/s. This diffusion coefficient is reflecting diffusion across the interphase of electrodes and electrolyte, and it is much lower compared to standard bulk electrolyte diffusion coefficients of 10^{-6} cm^2/s.

EIS Versus SOC; Charging and Discharging of a Cell

The internal resistance and AC impedance, as well as the various electrochemical parameters of a cell depend on the state-of-charge (SOC) and the temperature. Figure 12 shows the EIS data acquired at different SOC levels of a cylindrical cell, with the parameter R_{CT} changing most significantly over SOC.

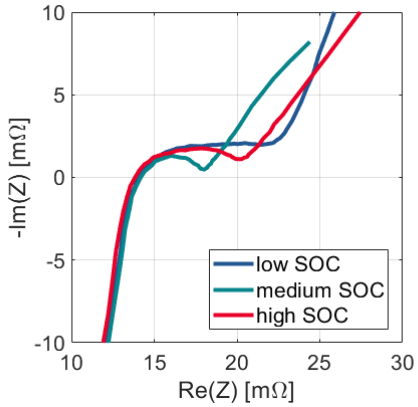

Figure 12. EIS curves of a cylindrical LIB cell acquired at different SOC levels, from 10 mHz to 10 kHz

As it could be seen, while there is monotonic decrease of R_{CT} with SOC when the SOC is increased from low values to medium values, the trend is reversed at higher SOC values. Therefore, to get consistent EIS data, the cells need to be charged to given SOC values before the EIS data is acquired. For this, charge and discharge cycles are used, and there are standard methods to discharge batteries over specific time-periods to test performance including rated capacity, capacity retention, effective internal resistance, discharge rate effect on capacity, life cycle performance, and extended overcharge. In the following, battery charging and discharging is further interpreted using the concepts of electrochemistry and EIS. During charging and discharging, the chosen voltage must be higher than the potential difference needed for lithiation and de-lithiation, respectively. Initially during charging, the voltage of the battery rises, then reaches a plateau, and at this point the current starts to drop due to limitation of diffusion. The battery is fully charged when the current drops to 3…5 % of the rated current and charging the battery further increases the risk of failure because of lithium plating, which compromises safety. For discharging the battery, the voltage signal drops and reaches the cut-off voltage where discharging should be stopped to avoid undesirable irreversible changes within the cell. For more details on the battery testing including charging & discharging, life cycles, and electronic loads please refer to the Keysight Application Note [7].

On the electrochemical process during charge/discharging, assume $LiCoO_2$ being the active material on the cathode and graphite being the anode material. Before charging, Lithium is in the oxidation state +1 and Cobalt in +3. During the charge process, Li^+ de-intercalates from the active material on the positive electrode (cathode) and Co^{3+} is oxidized to Co^{4+}. On the negative electrode (anode) Li^+ is inserted (intercalated) into the graphitized carbon on a conductive current collector, typically copper. The charge-transfer process occurs at the surface of the porous electrodes composed of graphite particles, and is related to the charge-transfer resistance R_{CT}. The electrolyte is typically an organic liquid (a Lithium salt, e.g. $LiPF_6$, in a mixture of a cyclic, e.g. propylene carbonate, and a linear carbonate, e.g. dimethyl carbonate). In the first charge/discharge forming cycles happening at the end of the production line, part of this electrolyte decomposes at the anode and forms the solid electrolyte interphase (SEI). The liquid electrolyte is aprotic because the voltage of the battery exceeds with 4V the water stability region both for cathode and anode. During battery discharge the current is carried by the Li^+ ions that move from the anode to the cathode and through the non-aqueous electrolyte and the separator. On the cathode, the transition-metals (e.g. Co^{2+}, Mn^{2+}) will be reduced. For the anode impedance spectrum, the diffusion impedance corresponds to a solid-state diffusion of Li^+ ions in graphite particles and follows the standard Warburg diffusion equation representing the mass transport inside a solid film. The impedance of the cathode is similar to that of anodes, being also composed of surface film, diffusion, and charge transfer impedance. While the SEI is formed on the anode during initial charge/discharge cycles, the electrolyte also reacts with the surface of the cathode, especially at high voltage, to generate a surface film, but this is less understood and not as dominant as the anode-SEI.

Conclusion

Several different cell chemistries are currently investigated in battery research labs. While on the one hand high energy density is required, the aspects of safety, lifetime, and thermal runaway get more and more important. All these requirements are currently tried to be met by very different approaches with different cell chemistry characteristics, including all solid-state cells, lithium-sulfur, Li-air (oxygen) and even non-Lithium systems like Na- or Mg-ion. The electrochemical methods presented here are indispensable in characterizing the various chemical systems. Also, EIS is used to classify cells based on their internal SOH and to select good cells from bad cells, which is particularly important for high-volume applications including high-power battery packs. In the work presented here, Keysight equipment is used to address this challenge at a very broad frequency range and with high sensitivity of few µΩ at ≥10 kHz measurement frequency. In general, three characteristic frequency regions can be identified in the EIS spectrum:

- The low frequency region (1 mHz…1 Hz) shows diffusion limited mass transport based on σ_W
- The higher frequency (1 Hz…1 kHz) is determined by the ratio of the Faradaic charge-transfer and capacitive double layer charging currents with the characteristic frequency
$$\omega_{RC} = 1/R_{CT}C_{CT}$$
- Above this critical frequency (1…10 kHz) the impedance is determined by the bulk-solution impedance (conductivity), as well as the resistance and the inductance of the wires and electrodes.

It has been shown that the frequency dependent complex impedance response of the batteries is used to differentiate between the different electrochemical and physical contributions, such as electrochemical reactions at the anode and cathode, physical phenomena (e.g. diffusion, electrode kinetics), or the capacitive and inductive properties of the system. Special attention must be given to ensure the stable and reliable operation of the EIS measurement to obtain high-quality data. With modern batteries that have low internal impedance values around 1 mΩ, current mode excitation (galvanostatic mode) is preferred and an accurate calibration is required to compare measurement results from different labs. For EIS calibration it was shown that adequate standards are required, and the definition of the standards should be as accurate as possible and most preferable the definition should be traceable to an accredited calibration laboratory. The results can be interpreted in terms of linear system theory, modeled as equivalent circuits, and checked for discrepancies with the Kramers-Kronig relations.

Acknowledgements

The work was carried out by Manuel Kasper and Ferry Kienberger (Keysight Labs - Linz), and Andrey Popov (Scienlab Test Solutions @ Keysight).

References

[1] *Basics of Measuring the Dielectric Properties of Materials*, Keysight Technologies, 2020.

[2] V. F. Lvovich, Impedance spectroscopy: Applications to Electrochemical and Dielectric Phenomena, Wiley, 2012, p. 368.

[3] A. Lasia, Electrochemical Impedance Spectroscopy and its Applications, Springer, 2014.

[4] Impedance Measurement Handbook: *A guide to measurement technology and techniques*, 6 ed., Keysight Technologies, 2016, p. 140.

[5] T. Osaka, T. Momma, D. Mukoyama and H. Nara, "Proposal of novel equivalent circuit for electrochemical impedance analysis of commercially available lithium ion battery," *Journal of Power Sources*, vol. 205, pp. 483-486, 2012.

[6] N. Meddings, M. Heinrich, F. Overney, J.-S. Lee, V. Ruiz, E. Napolitano, S. Seitz, G. Hinds, R. Raccichini, M. Gaberšček and J. Park, "Application of electrochemical impedance spectroscopy to commercial Li-ion cells: A review," *Journal of Power Sources*, vol. 480, 2020.

[7] *Battery Testing*, Keysight Technologies, 2017.

[8] A. J. Bard and L. R. Faulkner, Electrochemical Methods: Fundamentals and Applications, 2nd Edition, Wiley, 2000, p. 864.

[9] C. H. Hamann, A. Hamnett and W. Vielstich, Electrochemistry, 2 ed., Weinheim: Wiley-VCH, 2007, p. 532.